THE NATURE AND ORBIT OF THE OPHIUCHUS STREAM

Branimir Sesar[1,2], Jo Bovy[3,4], Edouard J. Bernard[5], Nelson Caldwell[6], Judith G. Cohen[7], Morgan Fouesneau[1], Christian I. Johnson[6], Melissa Ness[1], Annette M. N. Ferguson[5], Nicolas F. Martin[8,1], Hans-Walter Rix[1], Edward F. Schlafly[1], William S. Burgett[15], Kenneth C. Chambers[9], Heather Flewelling[9], Klaus W. Hodapp[9], Nick Kaiser[9], Eugene A. Magnier[9], Imants Platais[11], John L. Tonry[9], Christopher Waters[9], and Rosemary F. G. Wyse[11]

ABSTRACT

The Ophiuchus stream is the most recently discovered stellar tidal stream in the Milky Way (Bernard et al. 2014b). We present high-quality spectroscopic data for 14 stream member stars obtained using the Keck and MMT telescopes. We confirm the stream as a fast moving ($v_{los} \sim 290$ km s^{-1}), kinematically-cold group ($\sigma_{v_{los}} \lesssim 1$ km s^{-1}) of $\alpha-$enhanced and metal-poor stars ([α/Fe] ~ 0.4 dex, [Fe/H] ~ -2.0 dex). Using a probabilistic technique, we model the stream simultaneously in line-of-sight velocity, color-magnitude, coordinate, and proper motion space, and so determine its distribution in 6D phase-space. We find that that the stream extends in distance from 8 to 9.5 kpc from the Sun; it is 50 times longer than wide, merely appearing highly foreshortened in projection. The analysis of the stellar population contained in the stream suggests that it is ~ 13 Gyr old, and that its initial stellar mass was $\sim 2 \times 10^4$ $M_\odot$ (or at least $\gtrsim 4 \times 10^3$ $M_\odot$). Assuming a fiducial Milky Way potential, we fit an orbit to the stream which matches the observed phase-space distribution, except for some tension in the proper motions: the stream has an orbital period of ~ 360 Myr, and is on a fairly eccentric orbit ($e \sim 0.68$) with a pericenter of ~ 3.5 kpc and an apocenter of ~ 17.5 kpc. The phase-space structure and stellar population of the stream show that its progenitor must have been a globular cluster that was disrupted only ~ 250 Myr ago. We do not detect any significant overdensity of stars along the stream that would indicate the presence of a progenitor, and conclude that the stream is all that is left of the progenitor.

Subject headings: globular clusters: general — Galaxy: halo — Galaxy: kinematics and dynamics — Galaxy: structure

1. INTRODUCTION

One of the main goals of Galactic astronomy is the measurement of the Milky Way's gravitational potential, because knowledge of it is required in any study of the dynamics or evolution of the Galaxy. An important tool

[1] Max Planck Institute for Astronomy, Königstuhl 17, D-69117 Heidelberg, Germany
[2] Corresponding author: bsesar@mpia.de
[3] Institute for Advanced Study, Einstein Drive, Princeton, NJ 08540, USA
[4] John Bahcall Fellow
[5] SUPA, Institute for Astronomy, University of Edinburgh, Royal Observatory, Blackford Hill, Edinburgh EH9 3HJ, UK
[6] Harvard-Smithsonian Center for Astrophysics, 60 Garden Street, Cambridge, MA 02138, USA
[7] Division of Physics, Mathematics and Astronomy, California Institute of Technology, Pasadena, CA 91125, USA
[8] Observatoire astronomique de Strasbourg, Université de Strasbourg, CNRS, UMR 7550, 11 rue de l'Université, F-67000 Strasbourg, France
[9] Institute for Astronomy, University of Hawaii at Manoa, Honolulu, HI 96822, USA
[10] Department of Physics, Durham University, South Road, Durham DH1 3LE, UK
[11] Department of Physics and Astronomy, Johns Hopkins University, 3400 North Charles Street, Baltimore, MD 21218, USA
[12] Department of Astrophysical Sciences, Princeton University, Princeton, NJ 08544, USA
[13] US Naval Observatory, Flagstaff Station, Flagstaff, AZ 86001, USA
[14] Department of Physics, Harvard University, Cambridge, MA 02138, USA
[15] GMTO Corporation, 251 S. Lake Ave., Suite 300, Pasadena, CA 91101, USA

in this undertaking are stellar tidal streams, remnants of accreted Milky Way satellites that were disrupted by tidal forces and stretched into filaments as they orbited in the Galaxy's potential. The orbit of a stream is sensitive to the properties of the potential and thus can be used to constrain the potential over the range of distances spanned by the stream (e.g., Koposov et al. 2010; Newberg et al. 2010; Sesar et al. 2013; Belokurov et al. 2014). In this context, the recently discovered Ophiuchus stellar stream (Bernard et al. 2014b) is very interesting because it is located fairly close to the Galactic center (galactocentric distance of ~ 5 kpc), and as such probes the part of the potential that other known stellar tidal streams do not probe.

The Ophiuchus stream is a $\sim 2.5°$ long and $7'$ wide stellar stream that was recently discovered by Bernard et al. (2014b) in the Pan-STARRS1 photometric catalog (PS1; Kaiser et al. 2010). Bernard et al. inferred from its color-magnitude diagram that it is consistent with an old ($\gtrsim 10$ Gyr) and relatively metal-poor population ([Fe/H] ~ -1.3 dex) located ~ 9 kpc away at $(l, b) \sim (5°, +32°)$. They did not detect a progenitor (or a remnant of it), but suggested that the progenitor would most likely be a globular cluster.

Due to the lack of proper motion and line-of-sight velocity measurements, Bernard et al. could not determine the orbit of stream and thus could not use it to constrain the potential. Furthermore, without knowing the orbit of the stream, they could not fully explain two interest-

ing properties of the Ophiuchus stream, namely, its very short length and the lack of a visible progenitor. The projected angular length of 2.5° at a distance of ~ 9 kpc implies a projected physical length of ~ 400 pc for the Ophiuchus stream. Such as short length suggests that its progenitor must have been disrupted fairly recently. However, if that was the case, the progenitor should still be visible as an overdensity of stars somewhere along the stream. Yet, no progenitor has been detected so far.

To address the above questions, we need to know the orbit of the Ophiuchus stream, and to determine its orbit we need to measure the stream's line-of-sight velocity, distance, and proper motion. In Section 2, we describe the data we use in this work; the PS1 photometry and astrometry, the spectroscopic follow-up of candidate stream members, and the measurement of their line-of-sight velocities, element abundances, and proper motions. In Section 3, we provide a detailed characterization of the stream in position, velocity, and abundance (7-D) phase space. The constraints obtained in Section 3 are then used to constrain and examine the orbit of the stream (Section 4) and the time of disruption of its progenitor (Section 5). In Section 6, we discuss the nature of the stream's peculiar orbit, highlight the solved and uncovered puzzles related to the stream, and finally present our conclusions.

2. DATA

2.1. Overview of the Pan-STARRS1 survey

The PS1 survey has observed the entire sky north of declination $-30°$ in five filters covering $400 - 1000$ nm (Stubbs et al. 2010; Tonry et al. 2012). The 1.8-m PS1 telescope has a 7 deg^2 field of view outfitted with a billion-pixel camera (Hodapp et al. 2004; Onaka et al. 2008; Tonry & Onaka 2009). In single-epoch images, the telescope can detect point sources at a signal-to-noise ratio of 5 at 22.0, 22.0, 21.9, 21.0, and 19.8 mag in PS1 $grizy_{P1}$ bands, respectively. The survey pipeline automatically processes images and performs photometry and astrometry on detected sources (Magnier 2006, 2007). The uncertainty in photometric calibration of the survey is $\lesssim 0.01$ mag (Schlafly et al. 2012), and the astrometric precision of single-epoch detections is 10 milliarcsec (Magnier et al. 2008, hereafter mas).

2.2. Line-of-sight velocities

Based on the findings of Bernard et al. (2014b), we have used the dereddened and shifted fiducial of the old globular cluster NGC 5904 (from Bernard et al. 2014a) to select ~ 170 candidate Ophiuchus stream members from the PS1 photometric catalog. The candidates were observed using the DEIMOS spectrograph on Keck II (Faber et al. 2003) and using the Hectochelle fiber spectrograph on MMT (Szentgyorgyi et al. 2011) over a course of two nights.

Seven candidate blue horizontal branch stars were observed with DEIMOS on 2014 May 29$^{\text{th}}$ (project ID 2014A-C171D, PI: J. Cohen). The observations were made using the 0.8″ slit and the high resolution (1200G) grating, delivering a resolution of 1.2 Å in the 6250-8900 Å range. The spectra were extracted and calibrated

using standard IRAF[16] tasks. The uncertainty in the zero-point of wavelength calibration (measured using sky lines) was $\lesssim 0.04$ Å ($\lesssim 2$ km s^{-1} at 6563 Å).

The line-of-sight velocities of stars observed by DEIMOS were measured by fitting observed spectra with synthetic template spectra selected from the Munari et al. (2005) spectral library[17]. Prior to fitting, the synthetic spectra were resampled to the same Å per pixel scale as the observed spectrum and convolved with an appropriate Line Spread Function. The velocity obtained from the best-fit template was corrected to the barycentric system and adopted as the line-of-sight velocity, v_{los}. We added in quadrature the uncertainty in the zero-point of wavelength calibration (2 km s^{-1} at 6563 Å) to the velocity error from fitting.

The remaining 163 Ophiuchus stream candidates were observed with Hectochelle on 2014 June 6$^{\text{th}}$ (proposal ID 2014B-SAO-4, PI: C. Johnson). Observations were made using the RV31 radial velocity filter, which includes Mg I/Mgb features in the 5150-5300 Å range. To improve the signal-to-noise ratio (SNR) of faint targets, we binned the detector by 3 pixels in the spectral direction, resulting in an effective resolution of $R \sim 38,000$.

Hectochelle spectra were extracted and calibrated following Caldwell et al. (2009). To account for variations in the fiber throughput, the spectra were normalized before sky subtraction. The normalization factor was estimated using the strength of several night sky emission lines in the appropriate order. Sky subtraction was performed using the average of 20-30 sky fibers, using the method devised by Koposov et al. (2011). A comparison of observed and laboratory positions of sky emission lines did not reveal any significant offsets in wavelength calibration (i.e., no offsets greater than 0.5 km s^{-1} at 5225 Å).

The line-of-sight velocities of stars observed by Hectochelle were measured using the RVSAO package (Kurtz & Mink 1998), by cross-correlating observed spectra with a synthetic spectrum of an A-type and a G-type giant star (constructed by Latham et al. 2002). The velocity obtained from the best fitting template was adopted. To the uncertainty in v_{los}, measured by RVSAO, we added (in quadrature) the uncertainty in the zero-point of wavelength calibration, which we measured using sky emission lines to be 0.5 km s^{-1}. Finally, the measured velocities were corrected to the barycentric system using the BCV-CORR task.

A comparison of velocities measured from DEIMOS and Hectochelle spectra for star "bhb6" (Table 4), shows that the two velocity sets are consistent within stated uncertainties.

2.3. Element abundances

Even though the primary goal of spectroscopic observations was to obtain precise radial velocities, the wavelength range and the resolution of Hectochelle spectra are sufficient to allow estimates of element abundances.

We determined stellar parameters from the continuum-normalized, radial velocity-corrected spectra using the SMH code of Casey (2014), which is built on the MOOG code of Sneden (1973). Kurucz α−enhanced (0.4 dex)

---

[16] http://iraf.noao.edu/
[17] http://archives.pd.astro.it/2500-10500/

model atmospheres (Castelli & Kurucz 2004) and a line list compiled from Frebel et al. (2010) by Casey (2014) were used (see Table 5 in the electronic version of the Journal). First, effective temperatures were calculated from 2MASS photometry and color-temperature calibrations of González Hernández & Bonifacio (2009) and spectroscopic temperatures were optimized around this value using the SMH code, by removing abundance trends with line excitation potential. Parameters of $\log g$ and [Fe/H] were determined using 14 Fe I and 2-3 Fe II lines to achieve ionization balance, and microturbulence was calculated by removing abundance trends with reduced equivalent width of the lines. Estimates of the $\alpha-$enhancement were obtained using only the few available clean Mg, Ca and Ti (I and II) lines, which comprised a total of 6-8 lines per star. The abundances were measured from equivalent widths and the lines we used are listed in Table 5. Because Mg lines are strong and may be saturated, the values of [Mg/Fe] are significantly different than values of [Ca/Fe] and [Ti/Fe].

2.4. Proper motions

Proper motions are crucial constraints for determining the orbit of a stream (e.g., Koposov et al. 2010) To measure the proper motion of stars in the vicinity of the Ophiuchus stream, we combine the astrometry provided by USNO-B (Monet et al. 2003) and 2MASS (Skrutskie et al. 2006) catalogs with the PS1 catalog. The USNO-B catalog lists photometry and astrometry measured from photographic plates in five different band-passes (O, E, J, F, and N). The USNO-B plates were exposed at different epochs, and thus each object in the catalog can have a maximum of five recorded positions. The 2MASS catalog provides only one position entry per object.

To reduce the systematic offsets in astrometry between different catalogs, we first calibrate USNO-B and 2MASS positions to a reference frame that is defined by positions of galaxies observed in PS1 (which are on the ICRS coordinate system). We define galaxies as objects that have the difference between Point-Spread-Function (PSF) and aperture magnitudes in PS1 r_{P1} and i_{P1} bands between 0.3 and 1.0 mag.

The astrometric reference catalog is created by averaging out repeatedly observed positions of PS1 objects. Between May and June 2012, the region in the vicinity of the Ophiuchus stream was observed four times in PS1 g_{P1}, r_{P1}, and i_{P1} bands. To minimize the uncertainty in astrometry due to wavelength-dependent effects, such as the differential chromatic refraction (DCR), we only average out positions observed through the r_{P1}-band filter. Since the astrometric precision of single-epoch detections is 10 mas (Magnier et al. 2008), the precision of the average position is ~ 5 mas or better.

The USNO-B astrometry is calibrated following Munn et al. (2004, see their Section 2.1). First, we calculate the positions of objects at each of the five USNO-B epochs, using software kindly provided by J. Munn. Then, for each USNO-B object we find 100 nearest galaxies, calculate the median offsets in right ascension and declination between the reference PS1 position and the USNO-B position for these galaxies, and add the offsets to the USNO-B position in question. This is done separately for each of the five USNO-B epochs. The single-epoch 2MASS positions are calibrated using the same procedure.
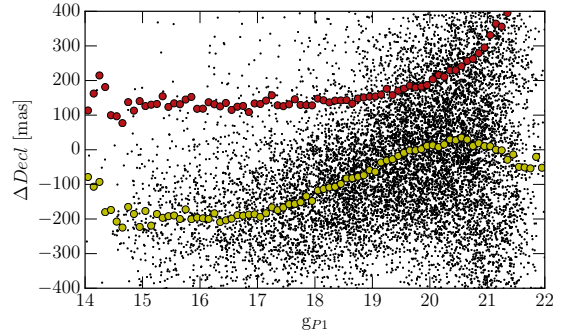
Figure 1. This plot illustrates the systematic offset in declination ($\Delta Decl$) of objects observed in the POSS-II Blue epoch of the USNO-B catalog (plate 799), as a function of the g_{P1}-band magnitude. For clarity, only a subset of objects are plotted. The solid yellow circles show the median $\Delta Decl$ in magnitude bins, and the solid red circles show the root-mean-square (rms) scatter in magnitude bins. Note how the brighter objects are systematically offset by ~ 200 mas from the fainter objects. The rms scatter indicates that the average precision in this coordinate and epoch is ~ 120 mas for objects brighter than $g_{P1} = 19$.

Having tied the positions for each object at one 2MASS and five USNO-B epochs to the PS1 astrometric reference frame, we can now check for any additional systematic uncertainties in the calibrated astrometry. We do so using the leave-one-out cross-validation. One of the six calibrated positions is withheld, and a straight line is fitted to the remaining five positions and the PS1 position. The straight line fit (i.e., essentially a proper motion fit, neglecting the parallax) is then used to predict the position of an object at the withheld epoch. The difference between the withheld position and the predicted position is labeled as ΔRA or $\Delta Decl$.

Inspection of ΔRA or $\Delta Decl$ values has revealed that the positions of USNO-B objects depend on magnitude for some epochs (e.g., see Figure 1). We have examined ΔRA and $\Delta Decl$ values in different regions of the sky, and have concluded that these astrometric issues affect individual photographic plates, and are not specific to a particular photographic bandpass. To remove this dependence, we subtract a plate-specific and magnitude-dependent offset (e.g., see yellow circles in Figure 1) from original USNO-B positions *before* we calibrate the positions using PS1 galaxies. Since USNO-B does not provide uncertainty in positions, we adopt the rms scatter of ΔRA and $\Delta Decl$ values (e.g., see red solid circles in Figure 1) as an estimate of the uncertainty in position at a given magnitude and epoch.

Finally, to measure the absolute proper motion of an object we fit a straight line to all available positions (min. 3, max. 7) as a function of time (the epoch baseline is 58 years). The proper motion of confirmed Ophiuchus stream members is listed in Table 4.

3. CHARACTERIZATION OF THE OPHIUCHUS STREAM

3.1. Line-of-sight velocities

The v_{los} distribution of stars observed by DEIMOS and Hectochelle is shown in Figure 2. In this Figure, a group of 14 stars with $285 < v_{los}/\mathrm{kms}^{-1} < 292$ clearly stands out. This group, which we identify as the Ophiuchus stream, is well-separated from the majority of stars which have $|v_{los}| < 200$ km s^{-1}. The positions, velocities, and PS1 photometry of stars in this group are listed in Table 4.
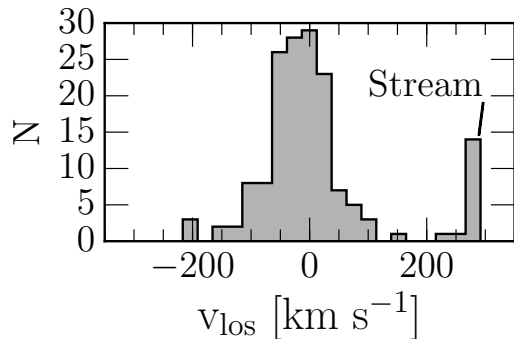
Figure 2. The distribution of heliocentric line-of-sight velocities of stars observed by DEIMOS and Hectochelle. The uncertainty in individual v_{los} measurements is $\lesssim 2$ km s^{-1} and the bin size is 25 km s^{-1}. The Ophiuchus stream is detected as a group of stars with $v_{los} \sim 290$ km s^{-1}.
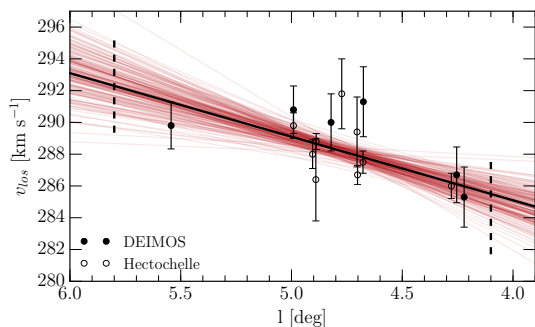
Figure 3. Line-of-sight velocities of stars in the Ophiuchus stream are shown as symbols with error bars. The thick solid line shows the most probable model ($v_{los}(l) = 4(l - 5) + 289.1$ km s^{-1}). To illustrate the uncertainty in the most probable model, the thin semi-transparent red lines show 200 models sampled from the posterior distribution. The vertical dashed lines show the likely extent of the stream (see Section 3.4).

A closer look at v_{los} of stars in the Ophiuchus stream (Figure 3) suggests that their velocities are changing as a function of galactic longitude. To fit this possible velocity gradient, we use an approach similar to the one taken by Martin & Jin (2010, see their Section 2.1.1).

We wish to find a set of parameters θ for which the observations of stars listed in Table 4, $\mathcal{D} = \{\mathbf{d_k}\}_{1 \leq k \leq 14}$, become most likely given the model we describe below. In the current problem, each data point $\mathbf{d_k}$ in data set $\mathcal{D}$ is defined by its galactic longitude and line-of-sight velocity, $\mathbf{d_k} = \{l_k, v_{los,k}\}$, and their associated uncertainties. The data points are also considered to be independent. The likelihood that these data points follow the model defined by the set of parameters θ, is then

$$\mathcal{L}(\mathcal{D}|\theta) = \prod_k \mathcal{L}_k(\mathbf{d_k}|\theta), \qquad (1)$$

where $\mathcal{L}_k(\mathbf{d_k}|\theta)$ is the likelihood of data point k to be generated from the model. Using Bayes Theorem, the probability of a model given the data, $P(\theta|\mathcal{D})$, is then

$$P(\theta|\mathcal{D}) \propto \mathcal{L}(\mathcal{D}|\theta)P(\theta), \qquad (2)$$

where $P(\theta)$ represents our prior knowledge on the model.

To model the velocity as a function of galactic longitude, we use the velocity gradient $\frac{dv_{los}}{dl}$, the velocity of the stream at galactic longitude $l = 5°$, $\overline{v_{los}}$, and the

Table 1
Element abundances of Ophiuchus stream stars

Name	T_{eff} (K)	$\log g$ (dex)	[Fe/H] (dex)	[Mg/Fe] (dex)	[Ca/Fe] (dex)	[Ti/Fe] (dex)
rgb1	5680	3.2	-2.00	-0.12	0.63	0.69
rgb2	5430	3.3	-1.95	0.06	0.62	0.47
rgb3	5700	3.1	-1.95	0.23	0.27	0.46
rgb4	5400	2.8	-1.90	0.24	0.57	0.42
rgb5	5720	2.9	-1.90	-0.14	0.83	—

Note. — The uncertainty in T_{eff} is < 200 K, < 0.45 dex for $\log g$, $\lesssim 0.2$ dex for [Fe/H], and ~ 0.35 dex for abundances of α−elements.

intrinsic velocity dispersion s as parameters. Given this model, the likelihood of a data point k is defined as

$$\mathcal{L}_k(l_k, v_{los,k}, \sigma_{v_{los,k}}|\overline{v_{los}}, \frac{dv_{los}}{dl}, s) = \mathcal{N}(v_{los,k}|v(l_k), \sigma_k'), \qquad (3)$$

where

$$\mathcal{N}(x|\mu, \sigma) = (1/\sqrt{2\pi\sigma^2})\exp(-0.5((x - \mu)^2)/\sigma^2) \qquad (4)$$

is a normal distribution, $v(l_k) = \frac{dv_{los}}{dl}(l_k - 5) + \overline{v_{los}}$ is the predicted velocity at galactic longitude l_k, and $\sigma_k' = \sqrt{s^2 + \sigma_{v_{los,k}}^2}$ is the quadratic sum of the intrinsic velocity dispersion and the uncertainty in line-of-sight velocity of data point k. The likelihood of all data points can then be calculated using Equation 1.

Before we can calculate the probability of a model, we need to define the prior probabilities of model parameters. As prior probabilities, we adopt priors that are uniform in these ranges: $270 < \overline{v_{los}}/\text{km s}^{-1} < 320$, $0 < \frac{dv_{los}}{dl}/\text{km s}^{-1} \text{deg}^{-1} < 8$, $0 \leq s/\text{km s}^{-1} < 3$.

To find the most probable model, we calculate Equation 2 over a fine three-dimensional grid in model parameters, and find values for which $P(\theta|\mathcal{D})$ is maximal. We find $\frac{dv_{los}}{dl} = 4 \pm 1$ km s^{-1} deg^{-1}, $\overline{v_{los}} = 289.1 \pm 0.5$ km s^{-1}, and a very small velocity dispersion of $s = 0.4^{+0.6}_{-0.3}$ km s^{-1}. The quoted uncertainties correspond to central 68% confidence limits (i.e., 1σ uncertainties). Thus, we detect a gradient in line-of-sight velocities at a 4σ level.

3.2. *Element abundances*

The preliminary element abundances of five (RGB) stars in the Ophiuchus stream (that is, the $v_{los} \sim 290$ km s^{-1} group), and observed by Hectochelle, are listed in Table 1. The uncertainties of the determined parameters are listed in the notes of Table 1.

We find the stars in the Ophiuchus stream to be poor in Fe ($[Fe/H] \sim -2.0$ dex) and enhanced in α-elements ($[\alpha/Fe] = 0.4 \pm 0.1$ dex). Their $[Fe/H]$ are consistent within 0.05 dex (root-mean-square scatter), despite fairly large estimated uncertainties in individual measurements ($\lesssim 0.2$ dex). The small scatter in $[Fe/H]$ suggests that these stars come from the same single stellar population.

Based on their position (within $5'$ of the Ophiuchus stream, as traced by Bernard et al. 2014b), kinematic and chemical properties, we conclude that all stars listed in Table 4 are high-probability members of the Ophiuchus stream.

3.3. *Color-magnitude diagram*

The sample of Ophiuchus stream members, which we have identified above using velocities and metallicities, now gives us an opportunity to further constrain the distance and the color-magnitude diagram (CMD) of the stream.

3.3.1. *Model*

To model the CMD of the stream, we use a probabilistic approach analogous to the one described in Section 3.1. In our data set, $\mathcal{D}$, each data point $\mathbf{d_k}$ is now defined by its galactic longitude and by its PS1 $grizy_{P1}$ magnitudes $\mathbf{d_k} = \{l_k, g_k, r_k, i_k, z_k, y_k\}$.

Our data set contains only the Ophiuchus stream stars that were identified based on spectroscopic data (i.e., velocity and metallicity). Thus, the set is uncontaminated but very sparse and has a complicated spatial selection function. Because of this, and because we are primarily interested in constraining the distance of the stream, we focus on finding the isochrone(s) that match the confirmed members in the color-magnitude space, and do not to model the projected shape of the stream on the sky (for now, but see Section 3.4).

To model the stream in color-magnitude space, we use a grid of theoretical PARSEC isochrones[18] (release v1.2S; Bressan et al. 2012; Chen et al. 2014). Each isochrone $\mathcal{I}$ provides PS1 magnitudes $m' = g'_{P1}, r'_{P1}, i'_{P1}, z'_{P1}, y'_{P1}$ for a single stellar population of age t, metal content Z, and parametrized for the mass-loss on the red giant branch using the variable values of the Reimers law parameter η (Reimers 1975, 1977). At galactic longitude $l = 5°$, the distance modulus of the stellar population is defined with parameter $\overline{DM}$, and a gradient in distance modulus with galactic longitude is modeled with parameter $\frac{dDM}{dl}$. The reddening is modeled by adding the $C_{ext}\left(\overline{E(B-V)} + \frac{dE(B-V)}{dl}(l-5)\right)$ term to isochrone magnitudes, where $\overline{E(B-V)}$ is the reddening at galactic longitude $l = 5°$ and $\frac{dE(B-V)}{dl}$ is a possible gradient in reddening. The extinction coefficients $C_{ext} = 3.172, 2.271, 1.682, 1.322, 1.087$ for PS1 $grizy$ bands were taken from Table 6 of Schlafly & Finkbeiner (2011).

To account for the fact that stellar evolution models are not perfect, we introduce a parameter σ_{iso} that models the uncertainty in PS1 $grizy$ magnitudes provided by PARSEC isochrones. In principle, one such parameter should be used for each band, as the uncertainty in models may propagate differently to different bands. We compared our results when a single σ_{iso} parameter is used for all bands, and when each band has its own model uncertainty. We have found that our results do not change significantly between these two cases, and have thus decided to use only one model magnitude uncertainty parameter for all bands (σ_{iso}) when modeling the color-magnitude diagram of the stream.

Given the above model of the stream, the likelihood of a data point k is

$$\mathcal{L}_k(\mathbf{d_k}|\mathcal{I}_k) = \int_{\mathcal{I}_k} \prod_{m=g,r,i,z,y} \mathcal{N}(m_k|m', \sigma'_{m_k})d\mathcal{I}_k, \quad (5)$$

[18] http://stev.oapd.inaf.it/cmd

where

$$\mathcal{I}_k = \mathcal{I}(l_k|age, Z, \eta, \overline{E(B-V)}, \frac{dE(B-V)}{dl}, \overline{DM}, \frac{dDM}{dl}, \sigma_{iso})$$
(6)

is the isochrone at the galactic longitude of data point k, $\mathcal{N}(x|\mu, \sigma)$ is a normal distribution, and $\sigma'_{m_k} = \sqrt{\sigma^2_{m_k} + \sigma^2_{iso}}$ is the sum of uncertainties in the isochrone magnitude (σ_{iso}) and the observed magnitude of data point k (σ_{m_k}). The likelihood of all data points can then be calculated by combining Equations 1 and 5. The integral in Equation 5 implies summation over an isochrone, that is, the observed $grizy_{P1}$ magnitudes are compared to predicted $grizy_{P1}$ magnitudes over the entire isochrone.

3.3.2. *Priors on the CMD model*

Before we can calculate the probability of a model, we need to define the prior probabilities of model parameters. Below, we list our priors and describe the justification for each one. A summary of priors is given in Table 2.

Based on spectroscopic data, the Ophiuchus stream is metal-poor ([Fe/H] $= -1.95 \pm 0.05$ dex) and $\alpha-$enhanced ([α/Fe] $= 0.4 \pm 0.1$ dex). As shown by Salaris et al. (1993), the $\alpha-$enhanced stellar population models are equivalent to scaled-solar ones with the same global metal content [M/H], where [M/H] for $\alpha-$enhanced models can be calculated using their Equation 3

$$[M/H] \approx [Fe/H] + \log_{10}(0.638 \times 10^{[\alpha/Fe]} + 0.362). \quad (7)$$

For the element abundance of the Ophiuchus stream, the above equation implies [M/H] $= -1.7 \pm 0.2$ dex. This means that we should adopt the normal distribution $\mathcal{N}(\log_{10}(Z/Z_\odot)|-1.7, 0.2)$ as the prior probability of metallicity Z (where $Z_\odot = 0.0152$ is the solar metal content used by this perticular set of PARSEC isochrones). However, in the context of cross-validating our analysis, we decided to replace the above metallicity prior in favor of a (less informative) prior that is uniform in the $0.0001 < Z < 0.0004$ range. Even though a less informative prior was adopted, at the end of Section 3.3.3 we find a very impressive consistency between the posterior distribution of metallicity Z (obtained using CMD fitting) and the spectroscopic estimate of Z (see bottom panel of Figure 4). In the end, it is important to note that our results would not have changed significantly if we used the more informative prior for metallicity content Z.

The presence of BHB stars, the [Fe/H] and the $\alpha-$enhancement of the stream point to an old stellar population. Thus, for age we adopt a uniform prior in the $8 < age/\text{Gyr} < 13.5$ range.

Metal-poor and old populations have $\eta \sim 0.4$ (Renzini & Fusi Pecci 1988). Therefore, for the mass-loss parameter η we adopt a uniform prior in the $0.2 < \eta < 0.5$ range. For the uncertainty in isochrone magnitudes, we adopt a prior that is uniform in the $0 \leq \sigma_{iso} < 0.1$ mag range.

Based on the inspection of Schlegel et al. (1998) and Schlafly et al. (2014) dust maps in the Ophiuchus region, we adopt uniform priors for the reddening at $l = 5°$ and its gradient: $0.1 < \overline{E(B-V)} < 0.3$ mag and

Table 2
Prior probabilities of CMD parameters

Parameter	Prior type	Range
Age	uniform	8 to 13.5 Gyr
Mass-loss parameter η	uniform	0.2 to 0.5
Metallicity Z	uniform	0.0001 to 0.0004
$\overline{E(B-V)}$	uniform	0.1 to 0.3 mag
$\frac{dE(B-V)}{dl}$	uniform	0 to 0.1 mag deg^{-1}
$\overline{DM}$	uniform	14.2 to 15.2 mag
$\frac{dDM}{dl}$	uniform	-0.5 to 0.5 mag deg^{-1}
σ_{iso}	uniform	0 to 0.1 mag

$0 \leq \frac{dE(B-V)}{dl} < 0.1$ mag deg^{-1}. According to Bernard et al. (2014b), the Ophiuchus stream is located about 9 ± 1 kpc from the Sun. Thus, for $\overline{DM}$ we adopted a uniform prior in the $14.2 < \overline{DM} < 15.2$ mag range (corresponding to the 7-11 kpc range). For the gradient in distance modulus, a uniform prior in the $|\frac{dDM}{dl}| < 0.5$ mag deg^{-1} range is adopted.

3.3.3. *Posterior distributions of CMD parameters*

To efficiently explore the parameter space, we use the Goodman & Weare (2010) Affine Invariant Markov chain Monte Carlo (MCMC) Ensemble sampler as implemented in the *emcee* package[19] (v2.1, Foreman-Mackey et al. 2013). We use 1000 walkers and obtain convergence[20] after a short burn-in phase of 100 steps per walker. The chains are then restarted around the best-fit value and evolved for another 4000 steps. We find that the marginal posterior distributions of parameters are quite Gaussian-like in shape, so we simply characterize their position using the median, and their width using the central 68% confidence limits (hereafter CL; see Table 3).

We find the stream to be 12.7 ± 0.4 Gyr old and to have a distance modulus of 14.68 ± 0.03 mag (i.e., a distance of 8.6 kpc) at galactic longitude $l = 5°$ (top panel of Figure 4). Most importantly, we detect a gradient of -0.23 ± 0.03 mag deg^{-1} in distance modulus. This gradient is inconsistent with zero (i.e., with the no gradient hypothesis) at a 7σ level, and agrees in sign with the Bernard et al. (2014b) conclusion that the eastern part of the stream is closer to the Sun (Figure 5). A comparison of CMDs of the Ophiuchus stream and field stars is shown in Figure 6. The CMD of field stars (grayscale pixels) was obtained by binning the $g_{P1} - i_{P1}$ colors and i_{P1}-band magnitudes of stars located more than $18'$ from the equator[21] of the Ophiuchus stream.

The gradient in distance modulus could be due to a gradient in reddening. However, while the two gradients are strongly anti-correlated (see Figure 7), they are still well-constrained by our data, as demonstrated by their 95% CLs that are narrower than their prior probability distributions (of $|\frac{dDM}{dl}| < 0.5$ mag deg^{-1} and $0 \leq \frac{dE(B-V)}{dl} < 0.1$ mag deg^{-1}, respectively).

In Section 3.3.2, we adopted a uniform prior for the metallicity content Z in order to test the predictive power

[19] http://dan.iel.fm/emcee/current/
[20] We checked for convergence of chains by examining the autocorrelation time of the chains per dimension.
[21] See Section 3 of Bernard et al. 2014b for its definition.

Table 3
Ophiuchus stream parameters

Parameter	Median and central 68% CL[a]
$\overline{v_{los}}$	289.1 ± 0.5 km s^{-1}
$\frac{dv_{los}}{dl}$	4 ± 1 km s^{-1} deg^{-1}
[Fe/H]	-1.95 ± 0.05 dex
$[\alpha/\text{Fe}]$	0.4 ± 0.1 dex
Age	12.7 ± 0.4 Gyr
Mass-loss parameter η	0.41 ± 0.02
Metallicity Z	$(2.3 \pm 0.2) \times 10^{-4}$
$\overline{E(B-V)}$	0.19 ± 0.01 mag
$\frac{dE(B-V)}{dl}$	0.04 ± 0.01 mag deg^{-1}
$\overline{DM}$	14.68 ± 0.03 mag
$\frac{dDM}{dl}$	-0.23 ± 0.03 mag deg^{-1}
σ_{iso}	0.015 ± 0.004 mag
l_{min}	$4.10^{+0.01}_{-0.08}$ deg
l_{max}	$5.80^{+0.05}_{-0.20}$ deg
A	31.369 ± 0.008 deg
B	$-0.73^{+0.01}_{-0.04}$
C	$-0.08^{+0.02}_{-0.05}$ deg^{-1}
Deprojected length	1.6 ± 0.3 kpc
σ_b	6 ± 1 arcmin
$\overline{\mu_l}$	-6.0 ± 0.4 mas yr^{-1}
$\frac{d\mu_l}{dl}$	-2.6 ± 0.9 mas yr^{-1} deg^{-1}
$\overline{\mu_b}$	2.3 ± 0.4 mas yr^{-1}
$\frac{d\mu_b}{dl}$	2.1 ± 0.8 mas yr^{-1} deg^{-1}
σ_{pm}	0.8 ± 0.5 mas yr^{-1}
N_{stars} ($i_{P1} < 20$)	193 ± 25 stars
Pericenter	3.50 ± 0.03^b kpc
Apocenter	17.5 ± 0.3 kpc
Eccentricity	0.67 ± 0.01
Orbital period	360 ± 5 Myr
Radial period	245 ± 3 Myr
Vertical period	356 ± 5 Myr
Mass of the progenitor	$\sim 2 \times 10^4$ $M_\odot$ ($> 4 \times 10^3$ $M_\odot$)

[a] The median and the central 68% confidence limits are measured from marginal posterior distributions.
[b] The uncertainties in orbital parameters do not account for the uncertainties in the assumed potential.

our dataset. As shown in the bottom panel of Figure 4, the peak of the marginal posterior distribution of Z is consistent with the mean value of Z estimated from spectroscopic data (solid vertical line), and the distribution is even narrower than the distribution of Z estimated from spectroscopy (dashed vertical lines). This result demonstrates the predictive power of our data. It shows how a combination of good coverage of the CMD, PS1 photometry, and detailed modeling can provide an accurate and precise estimate of the metallicity of single stellar populations.

3.4. *Modeling the proper motion and the extent of the stream*

The longitude-dependent CMD model we have built in Section 3.3, and the luminosity functions associated with the model, allow us to assign a likelihood that a star is a member of the Ophiuchus stream, based on the star's galactic longitude l, $g - i$ color, and i-band magnitude. The distribution of field stars in the $g - i$ vs. i color-magnitude diagram (grayscale pixels in Figure 6), on the other hand, enables us to estimate the likelihood that a star is associated with the field. As we show in this
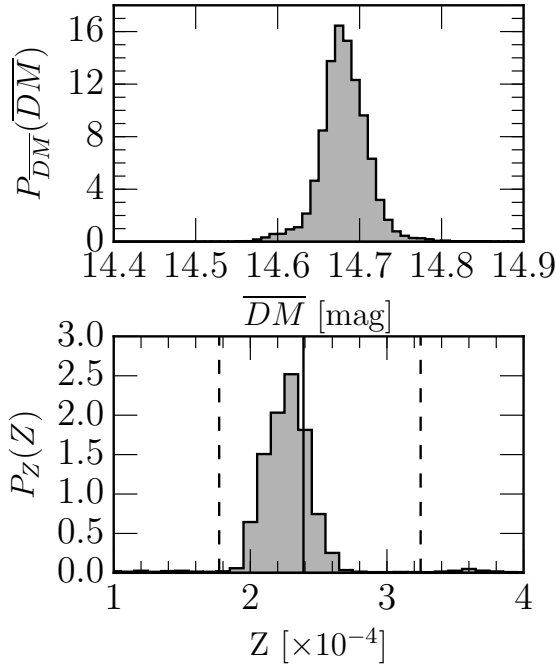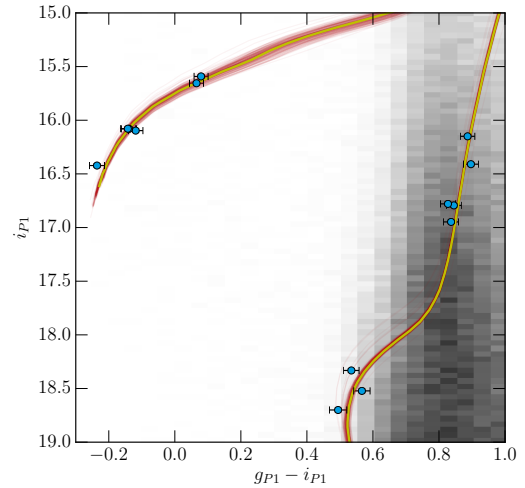
Figure 4. Marginal posterior distributions of distance modulus at $l = 5°$ (*top*) and metallicity Z (*bottom*). In the bottom panel, the solid vertical line shows the mean metallicity Z measured from spectroscopy ([Fe/H] $= -1.95 \pm 0.05$ dex, [α/Fe] $= 0.4 \pm 0.1$ dex), while the dashed lines show the uncertainty in the spectroscopic estimate of Z.
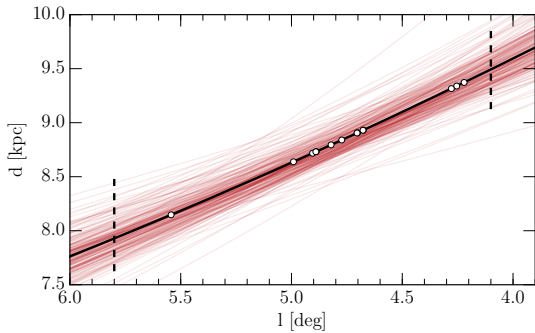

Figure 5. Heliocentric distance of the Ophiuchus stream as a function of galactic longitude l. The thick solid line shows the most probable model ($DM(l) = -0.23(l - 5) + 14.68$ mag). To illustrate the uncertainty in the most probable model, the thin semi-transparent red lines show 200 models sampled from the posterior distribution. The vertical dashed lines show the likely extent of the stream (see Section 3.4). The white circles plotted on top of the solid line show the positions of 14 confirmed stream members, where their distance modulus was calculated using the most probable model of $DM(l)$.

section, these two probability density functions, when combined with positional and proper motion data, can be used to simultaneously trace the extent of the Ophiuchus stream and determine its proper motions across the sky.

In principle, we could measure the proper motion of the Ophiuchus stream using the proper motion of its confirmed members. However, since our sample of confirmed members contains only 14 stars, there is a possibility that one or two stars with incorrectly measured proper motions may bias the results. As an example, stream member "rgb4" is clearly an outlier in proper motion as it has $\mu_l \sim -30$ mas yr^{-1}, while the remaining members

Figure 6. The $g_{P1} - i_{P1}$ vs. i_{P1} color-magnitude diagram showing the most probable isochrone (yellow thick line) and 200 isochrones randomly sampled from the stream's full posterior distribution (semi-transparent dark red thin lines). The isochrones have been shifted to match the distance of the stream at $l = 5°$. The grayscale pixels show the density distribution of field stars in this diagram (i.e., their probability density function). For illustration only, the color and magnitude of observed stars have been corrected for gradients in distance modulus and reddening, using median $\frac{dDM}{dl}$ and $\frac{dE(B-V)}{dl}$ values.
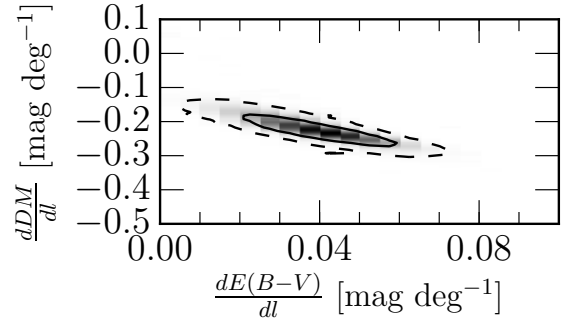
Figure 7. The joint posterior distribution of gradients in distance modulus and reddening (grayscale pixels). The 68% (1σ) and 95% (2σ) CL contours are shown as solid and dashed lines, respectively.

have $\mu_l \sim -6$ mas yr^{-1}. A visual inspection of digitized photographic plates has revealed that "rgb4" is blended with a neighbor of similar brightness, which affects the measured position of the star and its proper motion.

Fortunately, we do not need to rely only on confirmed members and can use a much larger sample of stars in the vicinity of the Ophiuchus stream to constrain its proper motion and extent. As we detail below, we use a probabilistic approach (see Sections 3.1 and 3.3) and model the distribution of stars simultaneously in coordinate, proper motion, and color-magnitude space as a mixture of stream and field (i.e., non-stream) stars. Even though we do not *a priori* know which star is a true member of the stream, we assume that as an ensemble, the stream stars have certain characteristics which make them distinguishable from field stars (e.g., common proper motion, distance, position on the sky and in the CMD), and that the *scatter* in these characteristics is sufficiently

small to overcome the fact that there are a lot more field than stream stars. The narrow width of the stream in color-magnitude (Figure 6) and coordinate space (Figure 1 of Bernard et al. 2014b) support this assumption. After all, if the stream did not have these characteristics, it likely would not have been detected by Bernard et al. (2014b) in the first place.

Even though the probabilistic approach we describe below uses all of the stars in the vicinity of the Ophiuchus stream to constrain the its extent and proper motion, we expect that most of the signal will come from main sequence turn-off (MSTO) stars associated with the stream. As shown in Figure 6, the stream's MSTO is bluer than the field population, which means that stars in this region of the color-magnitude diagram are much more likely to be associated with the stream than with the field population. Thus, the statistical weight of such stars will be greater than, for example, the weight of stream's RGB stars, which occupy the region of the color-magnitude diagram that is heavily dominated by field stars.

Assuming the stream extends between galactic longitudes l_{min} and l_{max}, the likelihood that a star with galactic longitude l_k, latitude b_k, proper motions in galactic coordinates of $\mu_{l,k}$ and $\mu_{b,k}$, color $(g-i)_k$ and magnitude i_k is drawn from the mixture model, is equal to

$$\mathcal{L}(\mathbf{d_k}|\theta) = f(l_k)\mathcal{L}(\mathbf{d_k}|\theta_{stream}) + (1 - f(l_k))\mathcal{L}(\mathbf{d_k}|\theta_{field}),$$
(8)

where $\mathbf{d_k} \equiv \{l_k, b_k, \mu_{l,k}, \mu_{b,k}, (g-i)_k, i_k\}$ contains measurements for data point (star) k, and $\theta \equiv \{\theta_{stream}, \theta_{field}\}$ contains parameters that model the distribution of stream and field stars, respectively. The parameter f specifies the fraction of stars in the stream (out of all stars between l_{min} and l_{max}) and is $f(l_k) \in [0,1]$ for $l_{min} < l_k < l_{max}$, otherwise, it is $f(l_k) = 0$.

The likelihood $\mathcal{L}(\mathbf{d_k}|\theta_{stream})$ is a product of spatial likelihood $\mathcal{L}(l_k, b_k|\theta_{stream}^{spatial})$, proper motion likelihood $\mathcal{L}(l_k, \mu_{l,k}, \mu_{b,k}|\theta_{stream}^{pm})$, and the color-magnitude likelihood $\mathcal{L}(l_k, (g-i)_k, i_k|\theta_{stream}^{CM})$

$$\mathcal{L}(\mathbf{d_k}|\theta_{stream}) = \mathcal{L}(l_k, b_k|\theta_{stream}^{spatial})$$
$$\times \mathcal{L}(l_k, \mu_{l,k}, \mu_{b,k}|\theta_{stream}^{pm})$$
$$\times \mathcal{L}(l_k, (g-i)_k, i_k|\theta_{stream}^{CM}).$$
(9)

The likelihood for field stars, $\mathcal{L}(\mathbf{d_k}|\theta_{field})$, has the same decomposition.

In galactic coordinates, the distribution of stream stars is modeled as a parabola along the stream, with a Gaussian width σ_b in the latitude direction, that is

$$\mathcal{L}(l_k, b_k|\theta_{stream}^{spatial}) = \mathcal{N}(b_k|\nu(l_k), \sigma_b),$$
(10)

where $\nu(l_k|A, B, C) = A + B(l_k - 5) + C(l_k - 5)^2$ is the galactic latitude of the equator of the stream. The spatial distribution of field stars is modeled as a straight line with a Gaussian width σ_b'

$$\mathcal{L}(l_k, b_k|\theta_{field}^{spatial}) = \mathcal{N}(b_k|\nu'(l_k), \sigma_b'),$$
(11)

where $\nu'(l_k|A', B') = A' + B'(l_k - 5)$.

At galactic longitude $l = 5°$, the stream is assumed to have proper motion $\overline{\mu_l}$ and $\overline{\mu_b}$, with possible gradients in proper motion of $\frac{d\mu_l}{dl}$ and $\frac{d\mu_b}{dl}$ (i.e., gradients as a function

of galactic longitude). The proper motion likelihood of stream stars is then

$$\mathcal{L}(l_k, \mu_{l,k}, \mu_{b,k}|\theta_{stream}^{pm}) =$$
$$\mathcal{N}(\mu_{l,k}|\mu_l(l_k), \sigma_k')$$
$$\times \mathcal{N}(\mu_{b,k}|\mu_b(l_k), \sigma_k'),$$
(12)

where $\mu_l(l_k) = \frac{d\mu_l}{dl}(l_k - 5) + \overline{\mu_l}$ and $\mu_b(l_k) = \frac{d\mu_b}{dl}(l_k - 5) + \overline{\mu_b}$ are the predicted proper motions of the stream at galactic longitude l_k, and $\sigma_k' = \sqrt{\sigma_{pm}^2 + \sigma_{\mu,k}^2}$ is the quadratic sum of the intrinsic proper motion dispersion and the uncertainty in the corresponding proper motion of data point k. The purpose of parameter σ_{pm} is to account for any additional scatter in proper motions (e.g., due to unaccounted errors). The proper motion likelihood of field stars has the same form (but different parameters) as the proper motion likelihood of stream stars.

The likelihood that a star is drawn from the stream's CMD is defined as

$$\mathcal{L}(l_k, (g-i)_k, i_k|\theta_{stream}^{CM}) = \zeta \int\int \mathcal{N}((g-i)_k'|g-i, \sigma_{(g-i)_k})$$
$$\times \mathcal{N}(i_k'|i, \sigma_{i_k})\mathcal{I}(g-i, i)d(g-i)di,$$
(13)

where $\sigma_{(g-i)_k}$ and σ_{i_k} are the uncertainty in color and magnitude of data point k, and ζ is a normalization constant calculated such that the integral of Equation 13 over the considered region of CM space is unity. To account for the gradient in reddening, $(g-i)_k' = (g-i)_k - 1.49\frac{dE(B-V)}{dl}(l_k - 5)$ and $i_k' = i_k - 1.682\frac{dE(B-V)}{dl}(l_k - 5) - \frac{dDM}{dl}(l_k - 5)$ are the $g_{P1} - i_{P1}$ color and i_{P1}-band magnitude of data point k offset by the difference in reddening between galactic longitudes l_k and $l = 5°$, where $\frac{dE(B-V)}{dl} = 0.04$ mag deg^{-1} is the most probable gradient in reddening (see Table 3). Note that magnitude i_k is also offset by the difference in distance modulus between galactic longitudes l_k and $l = 5°$ (to account for the gradient in DM), where $\frac{dDM}{dl} = -0.23$ mag deg^{-1}.

In Equation 13, $\mathcal{I}(g-i, i)$ is the probability density function (PDF) of the Ophiuchus stream in the $g_{P1} - i_{P1}$ vs. i_{P1} color-magnitude space at galactic longitude $l = 5°$. This PDF was constructed by sampling isochrones from the stream's CMD model (Section 3.3.3), multiplying them with their luminosity functions, and then summing them up in a binned $g_{P1} - i_{P1}$ vs. i_{P1} color-magnitude diagram. The likelihood that a star is drawn from the field CMD has the same form as Equation 13, except the PDF for the field stars is different (see grayscale pixels in Figure 6).

In total, our model contains 20 parameters. For all of the parameters, we have adopted uniform priors within certain bounds. The allowed ranges of model parameters were determined by examining positions and proper motions of confirmed members and other stars. In addition to adopted priors, we also require that the parameters satisfy following constraints:

- the spatial width of the stream must be smaller or equal than the width of the spatial distribution of field stars: $\sigma_b \leq \sigma_b'$
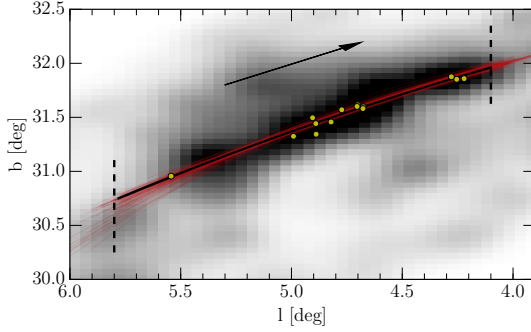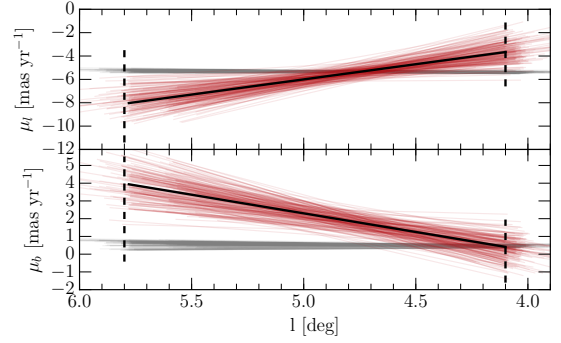
Figure 8. The extent of the Ophiuchus stream in galactic coordinates. The thick solid line shows the most probable model $(b(l) = 31.369 - 0.73(l - 5) - 0.08(l - 5)^2 \text{ deg})$ for the equator of the stream. To illustrate the uncertainty in the most probable model, the thin semi-transparent red lines show 200 models sampled from the posterior distribution. The vertical dashed lines show the likely extent of the stream (see Section 3.4). The yellow points show the positions of confirmed members and the arrow indicates the direction of movement of the stream. The gray-scale map shows the probability-weighted number density of likely Ophiuchus stream members, smoothed using a $6'$-wide Gaussian filter.

- the additional scatter in proper motion of stream stars must be smaller than the scatter in proper motions of field stars: $\sigma_{pm} \leq \sigma'_{pm}$, and

- the galactic latitudes of confirmed members (b_k^{conf}) must be within $3\sigma_b$ of the equator of the stream: $|\nu(l_k^{conf}) - b_k^{conf}| \leq 3\sigma_b$, where $\nu(l_k^{conf})$ is the galactic latitude of the stream at the position of confirmed members, and $1 \leq k \leq 14$.

As our data set, we use stars brighter than $i_{P1} = 20$ mag with measured proper motions, and located in a 2×2 deg^2 area centered on the Ophiuchus stream. To explore the parameter space, we use 200 *emcee* walkers and obtain convergence after a short burn-in phase of 100 steps. The chains are then restarted around the best-fit value and evolved for another 2000 steps. The median values and central 68% confidence limits of stream parameters are listed in Table 3.

We find the stream to be confined between galactic longitudes of 4.1 deg and 5.8 deg (Figure 8). When combined with the distance of the stream (Figure 5), this result implies that the deprojected length of the stream is 1.6 ± 0.3 kpc. Thus, the stream is very foreshortened in projection, by a ratio of 6 : 1. The galactic latitude of the equator of the stream is at $b_{stream}(l) = 31.369 - 0.73(l - 5) - 0.08(l - 5)^2$ deg, and the width of the stream is $\sigma_b = 6 \pm 1$ arcmin (in the galactic latitude direction). In direction perpendicular to the stream's equator, the stream is $\sim 3.5'$ wide, which is similar to width of $\sim 3'$ measured by Bernard et al. (2014b).

Based on a star's galactic longitude, color, magnitude, and proper motion, and given the model of the stream derived so far, we can evaluate its probability that it is a member of the Ophiuchus stream. We have done so for all of the stars in the vicinity of the Ophiuchus stream and have created a probability-weighted number density map, shown as grayscale pixels in Figure 8. An inspection of the number density map did not reveal a significant overdensity of stars along the stream that would indicate the presence of a progenitor.

Figure 9. Proper motion of the Ophiuchus stream, inferred from the ensemble of likely stream members. The panels show the proper motion in galactic longitude (*top*) and latitude directions (*bottom*), as a function of galactic longitude l. The thick solid lines show the most probable models $(\mu_l(l) = -2.6(l - 5) - 6.0 \text{ mas yr}^{-1}, \mu_b(l) = 2.3(l - 5) + 2.3 \text{ mas yr}^{-1})$. To illustrate the uncertainty in most probable models, the thin semi-transparent red lines show 200 models sampled from respective posterior distributions. For comparison, the semi-transparent gray lines show the proper motion of field stars. The vertical dashed lines show the likely extent of the stream (see Section 3.4).

Our data indicate that the proper motion of the stream changes as a function of galactic longitude (Figure 9). The gradients in proper motion are significant at $\gtrsim 2\sigma$ level, and while their absolute values are similar (~ 2 mas yr^{-1} deg^{-1}), the gradients have opposite signs. For comparison, the gradients in proper motions of field stars are consistent with zero at 1σ level ($\frac{d\mu'_l}{dl} = 0.12^{+0.05}_{-0.11}$ mas yr^{-1} deg^{-1} and $\frac{d\mu'_b}{dl} = 0.14^{+0.04}_{-0.13}$ mas yr^{-1} deg^{-1}). Overall, the proper motions of field stars are consistent with apparent motions of a population at ~ 9 kpc, due to the motion of the Sun around the Galaxy.

The stream parameters we have obtained so far can be used to place a lower limit on the mass of the initial population of the Ophiuchus stream. The fraction of stars f in the stream between longitudes l_{min} and l_{max}, can be converted to the number of stars in the stream, N_{stars}. We find that there are $N_{stars} = 193 \pm 25$ stars brighter than $i_{P1} = 20$ mag in the Ophiuchus stream. If we adopt the luminosity function associated with the most probable CMD model of the stream and assume Kroupa (1998) initial mass function (not corrected for binarity), this number of stars implies that the initial population of the Ophiuchus stream had to have a mass of at least $M_{init} = (4.0 \pm 0.5) \times 10^3 \, M_\odot$.

4. ORBIT OF THE OPHIUCHUS STREAM

The data and models of the stream obtained in previous sections now enable us to constrain the orbit of the Ophiuchus stream. For this purpose we use *galpy*[22], a package for galactic dynamics written in *Python* programming language (Bovy 2015).

To take full advantage of the stream constraints derived so far, we randomly draw 200 line-of-sight velocity, CMD, position, and proper motion models from posterior distributions obtained in previous sections, and perform orbit fitting on data sets created from these models. Each data set consists of 100 data points uniformly sampled in galactic longitude from l_{min} to l_{max}. Each data point is defined by its position and proper motion in galactic

---

[22] http://github.com/jobovy/galpy

coordinates, heliocentric distance, and line-of-sight velocity. To emulate the width of the stream, we assign an uncertainty of σ_b to positions of data points. To all data points we assign a 3% uncertainty in distance, 2 km s^{-1} uncertainty in velocity, and 2 mas yr^{-1} of uncertainty in proper motions. We have verified that our results do not change significantly if these uncertainties are changed. To convert the observed values into 3D positions and velocities, *galpy* assumes the circular velocity at the solar radius is 220 km s^{-1}, the Sun is located 8 kpc from the Galactic center, and Sun's motion in the Galaxy is (-11.1, 244, 7.25) km s^{-1} (Schönrich et al. 2010; Bovy et al. 2012).

The orbits are integrated in the default *galpy* potential, called MWPotential2014 (Table 1 of Bovy 2015). This potential consists of a bulge modeled as a power-law density profile that is exponentially cutoff with a power-law exponent of -1.8 and a cut-off radius of 1.9 kpc, a Miyamoto-Nagai disk, and a dark-matter NFW halo. MWPotential2014 is consistent with a large variety of dynamical constraints on the potential of the Milky Way, ranging from the bulge to the outer halo.

The line-of-sight velocities, heliocentric distances, positions, and proper motions predicted by *galpy* orbits are shown as thin semi-transparent blue lines in Figure 10. Overall, the observed and predicted mean values and gradients agree within uncertainties. This agreement is not trivial. While there is always an orbit that will fit a *single* star in some potential, the same is not true for a *stream* of stars. For example, given the observed gradients and mean values in proper motion, distance, and position, the observed gradient in line-of-sight velocity has to be positive, otherwise, there is a strong discrepancy with the velocity predicted by the most probable orbit. Similarly, the observed gradient in distance modulus has to have a negative sign, otherwise a good orbit fit cannot be achieved. The most noticeable disagreement is between observed and predicted proper motions (bottom right panel of Figure 10), with the observed proper motions having a steeper gradient (by about a factor of two). While this discrepancy is significant, the mean proper motion of the stream (towards the Galactic center and away from the plane) is consistent with the extent and orientation of the stream (i.e., curving towards the Galactic center and moving away from the plane). Thus, this discrepancy does not significantly affect the results presented below.

Figure 11 illustrates the orbit of the Ophiuchus stream in the past 370 Myr. We find that the stream has a relatively short orbital period of 360 ± 5 Myr, and a fairly eccentric orbit ($e = 0.67 \pm 0.01$), with a pericenter of 3.50 ± 0.03 kpc and an apocenter of 17.5 ± 0.3 kpc. About 10 Myr ago, the stream passed through its pericenter and now it is moving away from the Galactic plane and towards the center. Regarding uncertainties on orbital parameters, we note that they *do not* account for uncertainties in the assumed MWPotential2014 potential.

5. TIME OF DISRUPTION

In the Introduction, we said that the short length of the Ophiuchus stream suggests that its progenitor must have been disrupted fairly recently. As we have shown in Section 3.4, part of the reason the stream is so short *in projection*, is the viewing angle – we are observing the

stream almost end-on.

Even when the projection effects are taken into account, the deprojected length is still fairly short, only 1.6 kpc. For comparison, the second shortest stellar stream is the Pisces stream (Martin et al. 2013, also known as the Triangulum stream, Bonaca et al. 2012) with a length of ~ 5.5 kpc. Therefore, the length of the stream still suggests that the stream formed recently, that is, it suggests that the progenitor was recently disrupted.

As the progenitor of the Ophiuchus stream orbited the Galaxy, it would have experienced the tidal force of the Galactic potential. This force can strip stars from the progenitor and it could have been strong enough to completely disrupt the progenitor.

In order to examine the influence of the tidal force, we have calculated its magnitude as a function of time for the most probable orbit of the Ophiuchus stream. The magnitude of the tidal force was calculated by finding the largest eigenvalue of the following matrix

$$ J = \begin{pmatrix} \frac{d^2\Phi}{dR^2} & \frac{d^2\Phi}{dRdZ} \\ \frac{d^2\Phi}{dZdR} & \frac{d^2\Phi}{dZ^2} \end{pmatrix}, \tag{14} $$

where Φ is value of the *galpy* MWPotential2014 potential at the position of the progenitor, and R and Z are coordinates in the cylindrical galactocentric system. The result is shown in Figure 12.

We find that the tidal force is the strongest during pericenter+disk passages, and that the progenitor of the stream could have been disrupted during one of those passages. To find if the progenitor was disrupted during one of these passages, we can use *galpy*.

Given an orbit, the time of disruption t_{dis}, and the velocity dispersion of the progenitor σ_v, *galpy* can generate a mock stream using the modeling framework of Bovy (2014). Observationally, for a fixed σ_v, t_{dis} is proportional to the stream's length (i.e., older streams are longer). In Section 3.1, we measured $s = 0.4$ km s^{-1} as the velocity dispersion of the stream. We find that by setting σ_v to the same value, the *galpy* mock stream has a velocity dispersion $\tilde{s} \approx 0.4$ km s^{-1} $= s$. We further find that $t_{dis} \sim 170$ Myr provides a good match between the observed and mock streams (see Figure 13). While we do not perform an exhaustive search of the (σ_v, t_{dis}) parameter space, very different values of σ_v or t_{dis} produce values of $\tilde{s}$ or a total length that are not consistent with observations. This result, and the fact that there was a disk+pericenter passage 250 Myr ago, strongly suggest that the stream formed about 250 Myr ago (i.e., that the progenitor was disrupted at that time).

As shown by Sanders & Binney (2013), the velocity dispersion of the progenitor scales with the mass of the progenitor as $\sigma_v \propto M_{dyn}^{1/3}$. In *galpy*, the model used for stream generation was calibrated using a progenitor of mass $M_{dyn} = 2 \times 10^4$ $M_\odot$. The stream formed by the tidal disruption of this progenitor could be modeled with $\sigma_v = 0.365$ km s^{-1} (Bovy 2014). Using the above scaling relation and $\sigma_v = 0.4$ km s^{-1}, we find that the progenitor of the Ophiuchus stream had a mass of $M_{dyn} \sim 2 \times 10^4$ $M_\odot$.

It is important to note that *galpy* creates only the stream, and that stars associated with the progenitor are not part of the mock stream (i.e., are not shown in
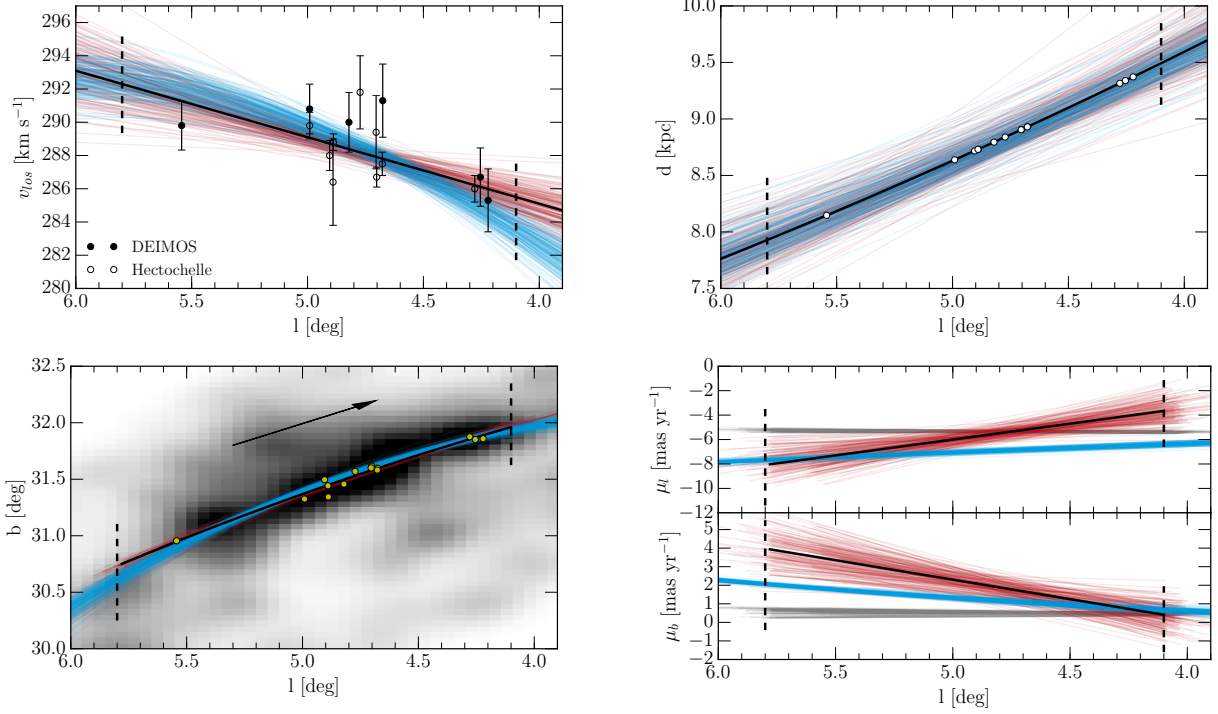
Figure 10. This plot compares line-of-sight velocities (*top left*), distances (*top right*), positions (*bottom left*), and proper motions (*bottom right*) calculated by *galpy* (thin blue lines) with models derived from observations (thin red lines). The observed and calculated values are consistent within uncertainties, with the exception of the proper motions, where the model cannot match the apparent gradient of the proper motions along the stream.
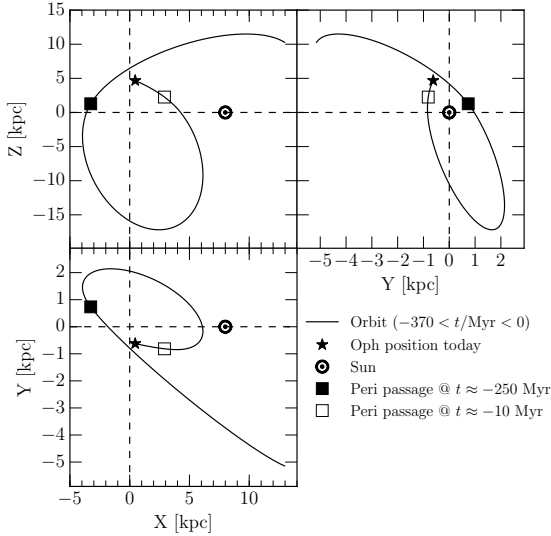
Figure 11. The orbit of the Ophiuchus stream in the past 370 Myr (about one orbital period), shown in a right-handed galactocentric Cartesian coordinate system. In this coordinate system, the Sun is at $(X, Y, Z) = (8, 0, 0)$ kpc and the y-axis is positive towards galactic longitude $l = 270°$. Note the pericenter passage at $t \approx -250$ Myr (solid square). Near this point in time, the stream was also passing through the disk ($Z \sim 0$ kpc, see the top left panel) and was experiencing strong tidal forces due to disk shocking (see Figure 12).

the middle panel of Figure 13). This is the reason an overdensity of stars (i.e., the progenitor) is not visible in the mock *galpy* stream.

To create a more realistic stream that includes a progenitor, we use the gyrfalcON code (Dehnen 2000, 2002) in the NEMO toolkit (Teuben 1995). We set up the
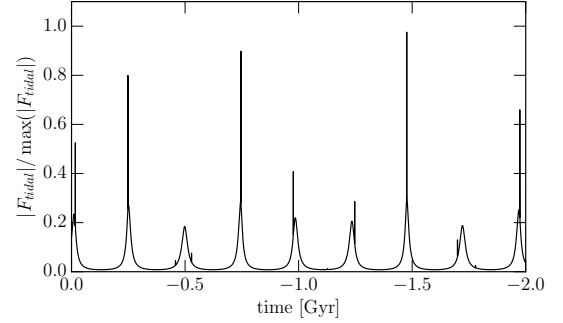
Figure 12. The tidal force acting on the Ophiuchus stream, normalized to the maximum tidal force in the past 2 Gyr. The narrow peaks correspond to passages through the disk (i.e., disk shocking, Ostriker et al. 1972) and the broader peaks correspond to passages through the pericenter.

progenitor as a King cluster (King 1966) with a mass of $1 \times 10^4 \, M_\odot$, tidal radius of 94 pc and a ratio of the central potential to the velocity dispersion squared of 2.0. The cluster is sampled using 20,000 particles and is evolved for ~ 375 Myr in the MWPotential2014 potential. The initial conditions are those at the $t \sim -375$ Myr apocenter of the most probable orbit of the Ophiuchus stream.

The number density map of the N-body stream created using gyrfalcON is shown in the bottom panel of Figure 13. The width and the length of the N-body stream match the observed stream fairly well. For comparison, if the cluster is evolved starting from the apocenter at $t \sim -870$ Myr, the resulting stream is much longer and inconsistent with observations. Based on this more realistic simulation, we conclude that the Ophiuchus stream likely formed about 250 Myr ago and that its progenitor was fully disrupted during a single disk+pericenter
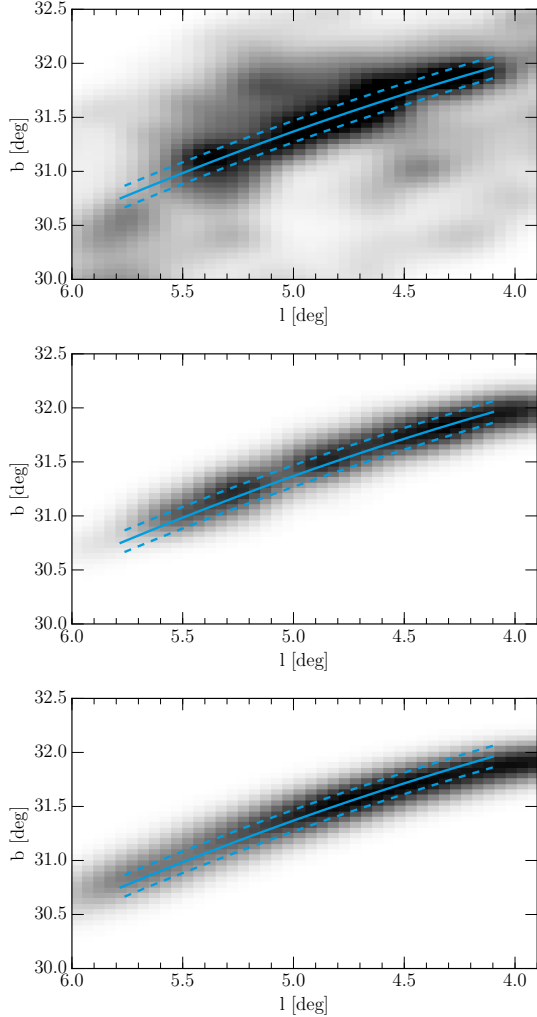
Figure 13. A comparison of the observed number density map of the stream (*top*), a map created from a mock stream generated using *galpy* (*middle*), and a map created from a N-body stream generated using NEMO. In all panels, the solid line shows the most probable position of the stream and the dashed lines illustrate its 1σ width. The mock *galpy* stream was generated assuming time of disruption $t_{dis} = 170$ Myr, and velocity dispersion $\sigma_v = 0.4$ km s^{-1}. Note a good agreement between the length and width of the observed, *galpy* and NEMO streams.

passage.

6. CONCLUSIONS AND SUMMARY

In this paper, we have presented follow-up spectroscopy and an astrometric and photometric analysis of the Ophiuchus stellar stream in the Milky Way, recently discovered by Bernard et al. (2014b) in PS1 data. We have been able to put together a comprehensive, empirical description of the Ophiuchus stream in phase space: we succeeded in determining the mean phase-space coordinates in all six dimensions, along with the gradients of those coordinates along the stream (see Table 3 for a summary of stream parameters).

Overall, phase-space data along the stream can be well matched by an orbit in a fiducial Milky Way potential: Ophiuchus is truly a thin and long (~ 1.6 kpc) stellar stream, 50 times longer than wide, that appears 6 : 1 foreshortened in projection; it is on a highly inclined orbit with only a 360 Myr orbital period; it is receding

from us at nearly 300 km s^{-1} and has just passed its pericenter at ~ 3 kpc from the Galactic center. This makes Ophiuchus the innermost stellar stream known in our Galaxy. It is also the only known kinematically-cold stellar stream to be seen nearly end-on.

The homogeneously metal-poor ([Fe/H] $= -2.0$ dex), α-enhanced ([α/Fe] ~ 0.4 dex) and old stellar population (~ 13 Gyr old), and the small line-of-sight velocity dispersion we found (< 1 km s^{-1}), strongly confirm the notion that the progenitor of the stream must have been a globular cluster. If the detected part of the stream encompasses most of the progenitor's stars, then the progenitor's tidal radius was ~ 90 pc and its mass was $\sim 2 \times 10^4$ $M_\odot$ (certainly greater than $\sim 4 \times 10^3$ $M_\odot$). In this respect, the Ophiuchus and the GD-1 stream (Grillmair & Dionatos 2006; Koposov et al. 2010) can be considered identical twins, as they have the same metallicity, the same mass, and no detectable progenitors.

Our analysis, however, leaves a number of questions open. First, the most probable orbit in the fiducial potential is not quite able to match the proper motions and their gradients along the stream. A thorough exploration whether there are axiymmetric or non-axisymmetric potentials that might be able to remedy this tension remains to be done. Alternatively, this discrepancy may indicate a problem with the proper motion data. While we have done our best to obtain good proper motions, we cannot fully dismiss this possibility. However, we expect that the proper motions provided by the the ongoing GAIA mission (Perryman et al. 2001) will resolve this discrepancy in the near future.

Second, the present analysis does not yet use the stream phase-space data to provide new constraints on the Galactic potential. In principle, Ophiuchus stream can provide constraints on the Galactic potential at about 5 kpc above the Galactic center, a location where few other constraints exist. As the top left panel of Figure 10 shows, the line-of-sight velocity of the stream is predicted to decrease to about 282 km s^{-1} at galactic longitude $l = 4°$. By measuring line-of-sight velocities of stars at this position, we can identify members of the Ophiuchus stream and test the assumed potential. Similarly, the potential may also be tested by identifying stream members at $l \gtrsim 5.8°$, where the stream is predicted to curve towards the galactic latitude $b = 30.5°$ (see the blue lines in the bottom left panel of Figure 10). By identifying stream members through line-of-sight velocities, we could also verify whether the "blobs" visible in the number density map (gray-scale map in the bottom left panel of Figure 10) are real or not (e.g., at $l = 4.3°$ and $l = 5.4°$). For example, such features may be related to overdensities caused by epicyclic movement of the tail stars (Küpper et al. 2012).

And finally, our analysis suggests that the progenitor of the stream was fully disrupted during a single disk+pericenter passage about 250 Myr ago. As N-body simulations show, this disruption was strong enough to smooth out the distribution of stars along the stream and effectively erase all evidence of the progenitor. If this scenario is correct, then the answer to the question "Where is the progenitor of the Ophiuchus stream?" is fairly simple – the Ophiuchus stream is all that is left of the progenitor.

While the above scenario seems to answer one question, it creates another one. The fact that the N-body stream ends up being too long if the cluster is evolved for more than ~ 400 Myr, suggests that the progenitor could not have been on the current orbit for more than ~ 400 Myr. If that is true, how did the progenitor end up on the current orbit and what was its original orbit? We expect that detailed N-body simulations will provide a more definitive answer to these questions and plan to pursue this approach.

REFERENCES

Belokurov, V., Koposov, S. E., Evans, N. W., et al. 2014, MNRAS, 437, 116

Bernard, E. J., Ferguson, A. M. N., Schlafly, E. F., et al. 2014a, MNRAS, 442, 2999

—. 2014b, MNRAS, 443, L84

Bonaca, A., Geha, M., & Kallivayalil, N. 2012, ApJ, 760, L6

Bovy, J. 2014, ApJ, 795, 95

—. 2015, ApJS, in press (arXiv:1412.3451)

Bovy, J., Allende Prieto, C., Beers, T. C., et al. 2012, ApJ, 759, 131

Bressan, A., Marigo, P., Girardi, L., et al. 2012, MNRAS, 427, 127

Caldwell, N., Harding, P., Morrison, H., et al. 2009, AJ, 137, 94

Casey, A. R. 2014, ArXiv e-prints

Castelli, F., & Kurucz, R. L. 2004, A&A, 419, 725

Chen, Y., Girardi, L., Bressan, A., et al. 2014, MNRAS, 444, 2525

Dehnen, W. 2000, ApJ, 536, L39

—. 2002, Journal of Computational Physics, 179, 27

Faber, S. M., Phillips, A. C., Kibrick, R. I., et al. 2003, in Society of Photo-Optical Instrumentation Engineers (SPIE) Conference Series, Vol. 4841, Instrument Design and Performance for Optical/Infrared Ground-based Telescopes, ed. M. Iye & A. F. M. Moorwood, 1657–1669

Foreman-Mackey, D., Hogg, D. W., Lang, D., & Goodman, J. 2013, PASP, 125, 306

Frebel, A., Simon, J. D., Geha, M., & Willman, B. 2010, ApJ, 708, 560

González Hernández, J. I., & Bonifacio, P. 2009, A&A, 497, 497

Goodman, J., & Weare, J. 2010, Commun. Appl. Math. Comput. Sci., 5, 65

Grillmair, C. J., & Dionatos, O. 2006, ApJ, 643, L17

Hodapp, K. W., Kaiser, N., Aussel, H., et al. 2004, Astronomische Nachrichten, 325, 636

Kaiser, N., Burgett, W., Chambers, K., et al. 2010, in Society of Photo-Optical Instrumentation Engineers (SPIE) Conference Series, Vol. 7733, Society of Photo-Optical Instrumentation Engineers (SPIE) Conference Series

King, I. R. 1966, AJ, 71, 64

Koposov, S. E., Rix, H.-W., & Hogg, D. W. 2010, ApJ, 712, 260

Koposov, S. E., Gilmore, G., Walker, M. G., et al. 2011, ApJ, 736, 146

Kroupa, P. 1998, MNRAS, 298, 231

Küpper, A. H. W., Lane, R. R., & Heggie, D. C. 2012, MNRAS, 420, 2700

Kurtz, M. J., & Mink, D. J. 1998, PASP, 110, 934

Latham, D. W., Stefanik, R. P., Torres, G., et al. 2002, AJ, 124, 1144

Magnier, E. 2006, in The Advanced Maui Optical and Space Surveillance Technologies Conference

Magnier, E. 2007, in Astronomical Society of the Pacific Conference Series, Vol. 364, The Future of Photometric, Spectrophotometric and Polarimetric Standardization, ed. C. Sterken, 153

Magnier, E. A., Liu, M., Monet, D. G., & Chambers, K. C. 2008, in IAU Symposium, Vol. 248, IAU Symposium, ed. W. J. Jin, I. Platais, & M. A. C. Perryman, 553–559

Martin, C., Carlin, J. L., Newberg, H. J., & Grillmair, C. 2013, ApJ, 765, L39

Martin, N. F., & Jin, S. 2010, ApJ, 721, 1333

Monet, D. G., Levine, S. E., Canzian, B., et al. 2003, AJ, 125, 984

Munari, U., Sordo, R., Castelli, F., & Zwitter, T. 2005, A&A, 442, 1127

Munn, J. A., Monet, D. G., Levine, S. E., et al. 2004, AJ, 127, 3034

Newberg, H. J., Willett, B. A., Yanny, B., & Xu, Y. 2010, ApJ, 711, 32

Onaka, P., Tonry, J. L., Isani, S., et al. 2008, in Society of Photo-Optical Instrumentation Engineers (SPIE) Conference Series, Vol. 7014, Society of Photo-Optical Instrumentation Engineers (SPIE) Conference Series

Ostriker, J. P., Spitzer, Jr., L., & Chevalier, R. A. 1972, ApJ, 176, L51

Perryman, M. A. C., de Boer, K. S., Gilmore, G., et al. 2001, A&A, 369, 339

Reimers, D. 1975, Memoires of the Societe Royale des Sciences de Liege, 8, 369

—. 1977, A&A, 61, 217

Renzini, A., & Fusi Pecci, F. 1988, ARA&A, 26, 199

Salaris, M., Chieffi, A., & Straniero, O. 1993, ApJ, 414, 580

Sanders, J. L., & Binney, J. 2013, MNRAS, 433, 1813

Schlafly, E. F., & Finkbeiner, D. P. 2011, ApJ, 737, 103

Schlafly, E. F., Finkbeiner, D. P., Jurić, M., et al. 2012, ApJ, 756, 158

Schlafly, E. F., Green, G., Finkbeiner, D. P., et al. 2014, ApJ, 789, 15

Schlegel, D. J., Finkbeiner, D. P., & Davis, M. 1998, ApJ, 500, 525

Schönrich, R., Binney, J., & Dehnen, W. 2010, MNRAS, 403, 1829

14

Sesar, B., Grillmair, C. J., Cohen, J. G., et al. 2013, ApJ, 776, 26

Skrutskie, M. F., Cutri, R. M., Stiening, R., et al. 2006, AJ, 131, 1163

Sneden, C. A. 1973, PhD thesis, THE UNIVERSITY OF TEXAS AT AUSTIN.

Stubbs, C. W., Doherty, P., Cramer, C., et al. 2010, ApJS, 191, 376

Szentgyorgyi, A., Furesz, G., Cheimets, P., et al. 2011, PASP, 123, 1188

Teuben, P. 1995, in Astronomical Society of the Pacific Conference Series, Vol. 77, Astronomical Data Analysis Software and Systems IV, ed. R. A. Shaw, H. E. Payne, & J. J. E. Hayes, 398

Tonry, J., & Onaka, P. 2009, in Advanced Maui Optical and Space Surveillance Technologies Conference

Tonry, J. L., Stubbs, C. W., Lykke, K. R., et al. 2012, ApJ, 750, 99

Table 4
Ophiuchus Stream Member Stars

Name	R.A. (deg)	Decl. (deg)	g_{P1} (mag)	r_{P1} (mag)	i_{P1} (mag)	z_{P1} (mag)	y_{P1} (mag)	v_{los} (km s^{-1})	DM (mag)	μ_l (mas yr^{-1})	(ma
bhb1	241.52271	-7.01555	16.05 ± 0.02	16.11 ± 0.02	16.22 ± 0.01	16.25 ± 0.02	16.25 ± 0.02	286.7 ± 1.8	$14.84^{+0.03}_{-0.02}$	-2.4 ± 2.0	(
bhb2	241.49994	-7.03409	16.02 ± 0.02	16.09 ± 0.02	16.21 ± 0.02	16.25 ± 0.02	16.23 ± 0.02	285.3 ± 1.9	$14.85^{+0.03}_{-0.03}$	-2.4 ± 1.8	−
bhb3	242.13551	-6.87785	15.96 ± 0.02	15.99 ± 0.01	16.11 ± 0.02	16.16 ± 0.02	16.13 ± 0.02	290.0 ± 1.8	$14.71^{+0.03}_{-0.02}$	-7.4 ± 2.0	
bhb4	241.94714	-6.88995	16.22 ± 0.02	16.32 ± 0.01	16.48 ± 0.02	16.54 ± 0.02	16.56 ± 0.02	291.3 ± 2.2	$14.74^{+0.03}_{-0.02}$	-4.3 ± 1.9	
bhb6	242.33018	-6.84405	15.67 ± 0.01	15.64 ± 0.01	15.59 ± 0.01	15.60 ± 0.02	15.54 ± 0.02	290.8 ± 1.5	$14.67^{+0.03}_{-0.02}$	-2.5 ± 1.8	(
bhb7	242.91469	-6.69329	15.66 ± 0.01	15.56 ± 0.02	15.57 ± 0.01	15.54 ± 0.02	15.50 ± 0.02	289.8 ± 1.5	$14.55^{+0.04}_{-0.03}$	-5.9 ± 2.0	
bhb6								289.8 ± 0.8			
rgb1	241.51689	-6.98511	17.71 ± 0.02	17.18 ± 0.02	16.91 ± 0.02	16.78 ± 0.02	16.71 ± 0.02	286.0 ± 0.8	$14.84^{+0.03}_{-0.03}$	-4.9 ± 2.0	−
rgb2	241.94649	-6.86113	17.34 ± 0.02	16.74 ± 0.02	16.46 ± 0.02	16.32 ± 0.02	16.25 ± 0.02	286.7 ± 0.6	$14.74^{+0.03}_{-0.02}$	-6.1 ± 2.1	
rgb3	241.96089	-6.89873	17.64 ± 0.02	17.08 ± 0.02	16.83 ± 0.02	16.68 ± 0.02	16.62 ± 0.02	287.5 ± 0.7	$14.74^{+0.03}_{-0.02}$	-6.5 ± 2.0	
rgb4	242.26139	-6.90190	17.05 ± 0.02	16.45 ± 0.02	16.17 ± 0.01	16.02 ± 0.02	15.93 ± 0.02	288.8 ± 0.5	$14.70^{+0.03}_{-0.02}$	-30.0 ± 1.8	−1
rgb5	242.14832	-6.79765	17.79 ± 0.02	17.23 ± 0.02	16.96 ± 0.02	16.82 ± 0.02	16.74 ± 0.02	288.0 ± 0.9	$14.69^{+0.03}_{-0.02}$	-6.8 ± 2.1	−
sgb1	241.95962	-6.86881	18.90 ± 0.02	18.53 ± 0.02	18.38 ± 0.02	18.31 ± 0.02	18.28 ± 0.02	289.4 ± 2.2	$14.74^{+0.03}_{-0.02}$	-6.5 ± 3.0	−
msto1	242.02040	-6.84122	19.22 ± 0.02	18.89 ± 0.02	18.74 ± 0.02	18.69 ± 0.02	18.62 ± 0.03	291.8 ± 2.2	$14.72^{+0.03}_{-0.02}$	-9.3 ± 3.2	(
msto2	242.18360	-6.84056	19.10 ± 0.02	18.70 ± 0.02	18.54 ± 0.02	18.45 ± 0.02	18.42 ± 0.03	286.4 ± 2.6	$14.70^{+0.03}_{-0.02}$	-6.1 ± 3.0	

Note. — The horizontal line separates stars observed by DEIMOS and Hectochelle. The name indicates the likely evolutionary stage inferred from isochro
The PS1 photometry is *not* corrected for extinction. The uncertainty in v_{los} includes the uncertainty from cross-correlation/fitting and the uncertainty in the zer
wavelength calibration. The DM indicates the average DM of the stream at the position of the star, and the uncertainties are 68% confidence limits. The proper
the galactic longitude direction, μ_l, includes the $\cos b$ term.